Fall Persistence Barrier of Sea Surface Temperature in the South China Sea Associated with ENSO*

JAU-MING CHEN[+]

Research and Development Center, Central Weather Bureau, Taipei, Taiwan

TIM LI

International Pacific Research Center, University of Hawaii at Manoa, Honolulu, Hawaii

CHING-FENG SHIH

Research and Development Center, Central Weather Bureau, Taipei, Taiwan

ABSTRACT

The authors investigate persistence characteristics of sea surface temperature (SST) in the South China Sea (SCS) in association with El Niño–Southern Oscillation (ENSO). It is found that a persistence barrier exists around October and November. This fall persistence barrier (FPB) is well recognized in the developing phase of strong ENSO cases, but becomes vague in weak ENSO and normal (non-ENSO) cases. During a strong El Niño developing year, salient features of the SCS SST anomaly (SSTA) associated with the FPB include a sign reversal between summer and winter and a rapid warming during fall. One possible cause of these SST changes, as well as the occurrence of the FPB, is the development and evolution of a low-level anomalous anticyclone (LAAC). The analyses show that the LAAC emerges in the northern Indian Ocean in early northern fall, moves eastward into the SCS during fall, and eventually anchors in the Philippine Sea in northern winter. This provides a new scenario for the generation of the anomalous Philippine Sea anticyclone previously studied. Its eastward movement appears to result from an east–west asymmetry, relative to the anticyclonic circulation center, of divergent flow and associated atmospheric vertical motion/moisture fields. The eastward passage of the LAAC across the SCS warms the underlying SST first via increased absorption of solar heating in October as it suppresses convective activities in situ, and next via decreased evaporative cooling in November and December as the total wind speed is weakened by the outer flows of the eastward-displacing LAAC. As such, the SCS SST changes quickly from a cold to a warm anomaly during fall, resulting in an abrupt change in anomaly patterns and the occurrence of the FPB. Analyses also suggest that the LAAC development during fall is relatively independent from the preceding Indian summer monsoon and the longitudinal propagation features of the ENSO-related Pacific SSTA. The aforementioned ocean–atmosphere anomalies contain an opposite polarity in a strong La Niña event. The low-level circulation anomaly weakens in intensity during weak ENSO cases and simply disappears during normal cases. As a result, the SCS FPB becomes indiscernible in these cases.

1. Introduction

One prominent feature of the ocean–atmosphere over the Pacific is the substantial decrease in forecast skills for El Niño–Southern Oscillation (ENSO) during spring (March–May) (e.g., Wright 1984; Cane et al. 1986; Latif and Graham 1992), reflecting the existence of a spring persistence barrier (SPB) in ENSO anomalies (e.g., Webster and Yang 1992). This feature has been found in observations and various types of coupled ocean–atmosphere model simulations (e.g., Zebiak and Cane 1987; Goswami and Shukla 1991; Webster and Yang 1992; Lau and Yang 1996), implicating the important role of ocean–atmosphere interaction processes in inducing this barrier. In spring, the seasonal cycle of the ocean–atmosphere over the Pacific is least robust, as revealed by the minimum east–west gradients in sea level pressure (SLP) and sea sur-

Corresponding author address: Dr. Jau-Ming Chen, Institute of Navigation Technology, National Kaohsiung Marine University, No. 482, Jhongjhou 3d Rd., Kaohsiung, 805, Taiwan.
E-mail: cjming@mail.nkmu.edu.tw

face temperature (SST) across the equatorial Pacific (Lau and Yang 1996). As such, the ocean–atmosphere becomes more sensitive to error growth induced by external noise associated with the highly variable Asian monsoon system (Webster and Yang 1992). The occurrence of the SPB is accompanied by rapid changes in monsoon-related anomalies and is regarded as resulting from phase locking of interannual anomalies to the annual variation of the tropical ocean–atmosphere (Lau and Yang 1996).

Ocean–atmosphere interaction processes in the Pacific are not only responsible for the occurrence of the SPB, but also for conveying the remote impacts of ENSO to SST variability in other tropical ocean basins (e.g., Meehl and Arblaster 2002; Li et al. 2005; Li and Wang 2005). Klein et al. (1999) showed that El Niño tended to induce a positive SST anomaly (SSTA) in the South China Sea (SCS) during its winter peak phase and the later seasons. The El Niño–related Pacific SSTA forced the east–west circulation to vary with a branch of anomalous subsidence over the SCS. This resulted in a decrease in cloud cover and an increase in solar radiation absorbed by the ocean, leading to anomalous warming in the SCS SST. From a different perspective, Wang et al. (2000) and Wang and Zhang (2002) found that El Niño was able to affect winter climate over the SCS and East Asia via an anomalous Pacific–East Asian teleconnection, featuring a low-level anomalous anticyclone centering in the Philippine Sea. This anticyclone induced anomalous southwesterly flows to weaken the prevailing winter northeasterly winds over the SCS and East Asia, leading to decreased latent heat flux and anomalous warming in these regions (e.g., Wang et al. 2000). These results illustrate a close linkage between ENSO and the SCS SSTA.

Variability of the ocean–atmosphere in the SCS region can exert noticeable impacts on the East Asian climate. After the onset of the SCS monsoon, water vapor originating from the SCS–tropical western Pacific regions is advected by monsoon southwesterlies toward East Asia to maintain the mei-yu and bai-u during June and July (Murakami 1959). On an interannual time scale, the ENSO-related Pacific SST in winter induces the longitudinal displacement of global wind anomalies to modulate the SCS SST (e.g., Ose et al. 1997; Klein et al. 1999). The resulting SSTA tends to persist from winter to the ensuing spring or summer (e.g., Lanzante 1996; Wang et al. 2000). The winter-to-summer SCS SST shows a close relationship with the ensuing summer monsoon rainfall in China (Shen and Lau (1995). Tomita and Yasunari (1996) and Ose et al. (1997) argued that the ENSO information in winter is likely passed to the following Asian summer monsoon via the

persistent SCS SSTA. In fact, Chinese researchers have included the winter information of ENSO to predict floods over China during the summer monsoon. The mechanism by which the SCS SSTA affects the East Asian summer monsoon is via a meridional wave train over East Asia and the western North Pacific excited by SST-associated convective anomalies over the SCS–Philippine Sea regions (e.g., Huang and Sun 1992; Wang and Fan 1999; Wang et al. 2001). Oceanic and atmospheric anomalies in the SCS region are important to variability, as well as prediction, of the East Asian climate.

It is apparent that a better understanding of the variability features of the ocean–atmosphere in the SCS region should benefit climate prediction tasks for East Asia. Based upon the dynamic relationships that exist among the SCS SSTA, ENSO, and the Pacific SPB reviewed above, some questions regarding the variability features of the SCS SST are raised as follows:

- Do the ENSO-related ocean–atmosphere interaction processes, which are largely responsible for the occurrence of the Pacific SPB, also cause a persistence barrier in the SCS SST?
- If yes, what are the major characteristics of this barrier? What is the relationship between this barrier and ENSO? Most importantly, what is the mechanism responsible for its occurrence?

The main purpose of this study is to investigate these questions. Its findings should enable us to better understand climate dynamics over East Asia, and better utilize the SCS SSTA in climate prediction systems for Asia.

2. Data

Two monthly-mean datasets for the period 1950–2000 are analyzed in this study. One dataset is the global SST data reconstructed with the empirical orthogonal functions method (Reynolds and Smith 1995; Smith et al. 1996) in a $2° \times 2°$ grid. The other dataset is the National Centers for Environmental Prediction–National Center for Atmospheric Research (NCEP–NCAR) reanalysis data (Kalnay et al. 1996). It includes wind, vertical motion, moisture, precipitation, and surface heating fields. The wind and vertical motion fields are in a $2.5° \times 2.5°$ grid, while the other fields are in $1.875°$ grid in longitude and 92 Gaussian grids in latitude.

3. Persistence characteristics of the SCS SST

Lau and Yang (1996) investigated ENSO's persistence characteristics in terms of autocorrelations of the

TABLE 1. Autocorrelation of the SCS SST index (area-mean averaging from the domain 10°–20°N, 110°–120°E) for the period 1950–2000 as functions of the 12 calendar months with lag time of 1–12 months. Autocorrelation values significant at the 95% level (≥0.28) are in bold font.

	Jan	Feb	Mar	Apr	May	Jun	Jul	Aug	Sep	Oct	Nov	Dec
Jan												
Feb	**0.73**											
Mar	**0.65**	**0.79**										
Apr	**0.64**	**0.71**	**0.79**									
May	**0.6**	**0.54**	**0.52**	**0.59**								
Jun	**0.62**	**0.47**	**0.49**	**0.54**	**0.66**							
Jul	**0.6**	**0.41**	**0.5**	**0.56**	**0.63**	**0.78**						
Aug	**0.56**	**0.45**	**0.46**	**0.49**	**0.57**	**0.69**	**0.75**					
Sep	**0.47**	**0.44**	**0.44**	**0.43**	**0.46**	**0.56**	**0.63**	**0.77**				
Oct	0.27	0.23	0.27	**0.34**	**0.33**	**0.44**	**0.43**	**0.48**	**0.57**			
Nov	0.05	0.1	0.16	0.12	0.15	0.23	0.25	0.27	**0.3**	**0.69**		
Dec	0.01	0.05	0.11	0.06	0.11	**0.3**	0.17	0.2	0.14	**0.48**	**0.77**	
Jan	−0.06	0.05	0.06	0.04	0.1	0.26	0.22	0.18	0.23	**0.44**	**0.63**	**0.79**
Feb		0.05	0.08	0.12	0.1	0.19	0.27	0.2	**0.28**	**0.44**	**0.48**	**0.56**
Mar			0.16	0.25	0.24	**0.3**	**0.37**	0.22	**0.3**	**0.41**	**0.5**	**0.5**
Apr				0.14	0.12	0.23	0.26	0.25	**0.34**	**0.43**	**0.52**	**0.55**
May					−0.1	0.13	0.09	−0.02	0.07	**0.38**	**0.35**	**0.49**
Jun						0.19	0.12	0.06	0.16	**0.34**	**0.3**	**0.49**
Jul							0.14	0.23	0.17	**0.34**	**0.32**	**0.46**
Aug								0.15	0.12	**0.38**	**0.41**	**0.52**
Sep									**0.3**	**0.46**	**0.38**	**0.53**
Oct										**0.45**	**0.39**	**0.42**
Nov											0.06	0.1
Dec		95% significance level = 0.28										0.04

Niño-3 SST index. For the SCS, an area-mean SST index averaging from the domain 10°–20°N, 110°–120°E was employed by Chen et al. (2003) to study the basin-scale ocean–atmosphere interaction processes associated with annual variation of the SCS SST. Autocorrelations of this SST index for the period 1950–2000 are used to diagnose the persistence characteristics of the SCS SST (Table 1). Autocorrelation values significant at the 95% level (≥0.28) are highlighted. The length of the highlighted column for a particular month can be regarded as a measure of SST memory starting from that month (Lau and Yang 1996). The SCS SST starting from January to August contains a persistent memory until September or October and seems to encounter a major barrier in fall (October or November). SST memory starting from September exhibits an oscillatory feature, while that starting from October to December persists for 10–12 months before it is interrupted by a barrier in November of the next year. These results clearly manifest that the SCS SST in winter, spring, and summer is statistically independent from the SST in the ensuing fall and the later seasons. The SCS SST tends to have a persistence barrier in fall. Another way to justify the existence of a persistence barrier is to use Webster and Yang's (1992) criterion, that is, if the autocorrelation halves from one month to another. An examina-

tion of Table 1 reveals that, regardless of the starting month, autocorrelation in November is about half or less in value of that in October. This result supports the argument that there is a fall persistence barrier (FPB) in the SCS SST.

To examine the relationship between the SCS FPB and ENSO, the ENSO cases are stratified into three categories according to the intensity of the winter [December–February (DJF)] Niño-3 SST index: the year assigned to each winter is the one including January and February. The assigned year and its previous one year are referred to as year (0) and year (−1), respectively. A year in which the winter Niño-3 SST index contains intensity larger than 1.0 standard deviation (SD) of its 1951–2000 time series is categorized as a strong ENSO case, between 0.5 and 1.0 SD as a weak ENSO case, and smaller than 0.5 SD as a normal (non ENSO) case (Table 2). Autocorrelations of the SCS SST index for these three cases all have the starting months in year (−1), that is, prior to the winter mature ENSO phase. For strong ENSO cases (Table 3), SST memory starting from January to September shows a major break around October and November, while that starting from October to December has a continuous memory throughout the following winter and spring. Clearly, there is a well-defined FPB in the SCS SST

TABLE 2. Member years of strong ENSO, weak ENSO, and normal cases.

Strong ENSO	El Niño	1958, 1966, 1969, 1973, 1983, 1987, 1992, 1995, 1998
	La Niña	1955, 1956, 1971, 1974, 1976, 1989, 1999, 2000
Weak ENSO	El Niño	1959, 1964, 1970, 1977, 1978, 1980, 1988, 1991, 1993
	La Niña	1951, 1963, 1965, 1968, 1972, 1975, 1985, 1996
Normal	Positive	1952, 1953, 1954, 1982, 1990, 1994
	Negative	1957, 1960, 1961, 1962, 1967, 1979, 1981, 1984, 1986, 1997

during the strong ENSO developing year. For weak ENSO (Table 4) and normal cases (Table 5), the SCS SST, regardless of the starting month, has a short memory less than 3 months and the memory can be disrupted in any month. The FPB of the SCS SST becomes vague in these two cases.

Is the FPB robust in the SCS region? Autocorrelations of a larger-area SCS SST index (4°–22°N, 110°–120°E, almost the entire SCS between the Indochina and the Philippines) are computed for all cases and strong ENSO cases. Their temporal features (not shown) are relatively consistent with those obtained with the original SST index. This insensitivity to the analysis domain implicates the robustness of the FPB in the SCS region. Our analyses also show that the SCS FPB tends to be significant in accordance with the increased ENSO strength. Clarke and Van Gorder (1999) and Yu (2005) found the ENSO–Pacific SPB relationship to be such that the SPB is consistently strong (weak) when biennial ENSO variability is large (small). The physical processes determining the ENSO–SCS FPB relationship need to be clarified.

4. Annual variation of the SCS ocean–atmosphere

The Pacific SPB results from interactions between annual and interannual anomalies of the tropical ocean–atmosphere (Lau and Yang 1996). Both the an-

TABLE 3. Autocorrelations of the SCS SST index for strong ENSO cases. The starting month is in year (−1). Autocorrelation values significant at the 95% level (≥0.49) are in bold font.

		Year (−1)											
		Jan	Feb	Mar	Apr	May	Jun	Jul	Aug	Sep	Oct	Nov	Dec
Yr (−1)	Jan												
	Feb	**0.9**											
	Mar	**0.79**	**0.88**										
	Apr	**0.89**	**0.88**	**0.86**									
	May	**0.72**	**0.76**	**0.74**	**0.79**								
	Jun	**0.76**	**0.62**	**0.66**	**0.73**	**0.8**							
	Jul	**0.73**	**0.64**	**0.69**	**0.72**	**0.79**	**0.9**						
	Aug	**0.63**	**0.64**	**0.67**	**0.65**	**0.73**	**0.8**	**0.87**					
	Sep	**0.54**	**0.69**	**0.75**	**0.68**	**0.68**	**0.63**	**0.76**	**0.83**				
	Oct	0.43	0.48	0.47	**0.55**	0.48	**0.52**	**0.51**	0.4	**0.66**			
	Nov	0.07	0.19	0.14	0.19	0.28	0.2	0.14	0.12	0.26	**0.77**		
	Dec	−0.02	−0.03	0.01	0.15	0.19	0.34	0.18	0.1	0.13	**0.66**	**0.81**	
Yr (0)	Jan	0.01	0.06	0.06	0.2	0.14	0.27	0.25	0.23	0.36	**0.71**	**0.71**	**0.85**
	Feb		0.06	0.03	0.13	0.07	0.22	0.23	0.27	0.32	**0.66**	**0.69**	**0.81**
	Mar			−0.04	0.11	−0.03	0.07	0.16	0.23	0.27	**0.6**	**0.65**	**0.67**
	Apr				0.16	−0.04	−0.02	0.08	0.14	0.29	**0.55**	**0.59**	**0.63**
	May					−0.22	0.01	0.05	−0.07	0.07	**0.49**	0.47	**0.6**
	Jun						0.1	0.1	−0.01	0.2	**0.58**	0.43	**0.63**
	Jul							0.03	0.01	0.18	0.47	0.41	**0.58**
	Aug								−0.08	−0.01	0.42	0.43	**0.63**
	Sep									0.14	**0.49**	0.38	**0.59**
	Oct										**0.58**	**0.51**	**0.65**
	Nov											0.46	**0.53**
	Dec			95% significance level = 0.49									**0.59**

TABLE 4. As in Table 3 except for weak ENSO cases. Autocorrelation values significant at the 95% level (≥0.49) are in bold font.

		Jan	Feb	Mar	Apr	May	Jun	Jul	Aug	Sep	Oct	Nov	Dec
Yr (−1)	Jan												
	Feb	**0.7**											
	Mar	**0.51**	**0.77**										
	Apr	0.48	**0.62**	**0.79**									
	May	0.45	0.23	0.39	**0.51**								
	Jun	**0.56**	0.29	**0.52**	**0.61**	**0.73**							
	Jul	**0.57**	0.39	**0.53**	**0.66**	**0.8**	**0.75**						
	Aug	0.4	0.26	0.4	0.46	**0.56**	**0.71**	**0.69**					
	Sep	0.42	0.28	0.34	0.28	0.24	**0.59**	0.43	**0.55**				
	Oct	0.12	−0.14	0.14	0.18	0.39	0.44	**0.52**	**0.54**	0.2			
	Nov	−0.06	−0.17	0.08	0.04	0.26	0.3	**0.49**	0.42	0.26	**0.7**		
	Dec	−0.12	−0.13	0.14	0.06	0.34	0.43	0.39	**0.67**	0.38	**0.64**	**0.78**	
Yr (0)	Jan	−0.26	−0.05	0.16	0.05	0.28	0.33	0.24	0.47	0.33	0.38	**0.62**	**0.86**
	Feb		0.08	0.25	0.24	0.08	0.02	0.29	0.32	0.38	0.33	0.43	0.48
	Mar			0.46	0.46	0.45	0.34	**0.59**	0.38	0.38	0.34	**0.6**	**0.56**
	Apr				0.23	0.27	0.15	0.3	0.21	0.34	0.18	**0.49**	0.44
	May					0.27	0.2	0.05	0.1	0.22	0.42	0.25	0.41
	Jun						0.44	0.32	0.41	0.31	0.09	0.18	0.4
	Jul							0.37	**0.6**	0.2	0.24	0.31	**0.53**
	Aug								**0.62**	0.37	0.43	0.47	**0.54**
	Sep									**0.66**	**0.56**	**0.61**	**0.63**
	Oct										−0.11	0.12	−0.07
	Nov											−0.42	−0.38
	Dec			95% significance level =0.49									−0.6

TABLE 5. As in Table 3 except for normal cases. Autocorrelation values significant at the 95% level (≥0.51) are in bold font.

|		Jan	Feb	Mar	Apr	May	Jun	Jul	Aug	Sep	Oct	Nov	Dec
Year (−1)	Jan												
	Feb	0.3											
	Mar	**0.52**	**0.59**										
	Apr	0.26	0.36	**0.59**									
	May	0.42	0.36	0.32	0.4								
	Jun	0.28	0.09	−0.09	−0.02	0.27							
	Jul	0.24	−0.31	−0.19	0.02	0.16	**0.54**						
	Aug	0.49	0.07	0.1	0.28	0.21	0.48	**0.6**					
	Sep	0.31	−0.04	−0.08	0.14	0.16	0.39	**0.55**	**0.8**				
	Oct	−0.07	0.01	0.03	0.2	−0.1	0.29	0.19	**0.55**	**0.72**			
	Nov	−0.03	−0.05	0.09	−0.1	−0.33	0.04	0.07	0.4	0.37	**0.57**		
	Dec	−0.01	0.02	0.09	−0.24	−0.39	0.02	−0.13	−0.03	−0.16	0.02	**0.68**	
Year (0)	Jan	−0.19	−0.1	−0.1	−0.36	−0.32	0.14	0.15	−0.23	−0.19	−0.05	0.5	**0.64**
	Feb		−0.31	−0.12	−0.09	0.04	0.3	0.32	−0.1	0.01	0.17	0.13	0.14
	Mar			−0.1	0.03	0.31	0.48	0.4	−0.07	0.19	0.17	−0.11	0
	Apr				−0.24	0.08	**0.59**	0.46	0.37	0.33	0.4	0.21	0.22
	May					−0.28	0.49	0.24	0.12	−0.09	0.2	0.23	0.48
	Jun						0.12	0.01	−0.18	−0.12	0.11	0.25	0.31
	Jul							0.19	0.25	0.12	0.14	0.05	−0.03
	Aug								0.15	−0.05	0.17	0.35	0.14
	Sep									0.25	0.16	0.03	0.19
	Oct										**0.58**	0.38	0.14
	Nov											−0.21	−0.38
	Dec			95% significance level = 0.51									−0.27
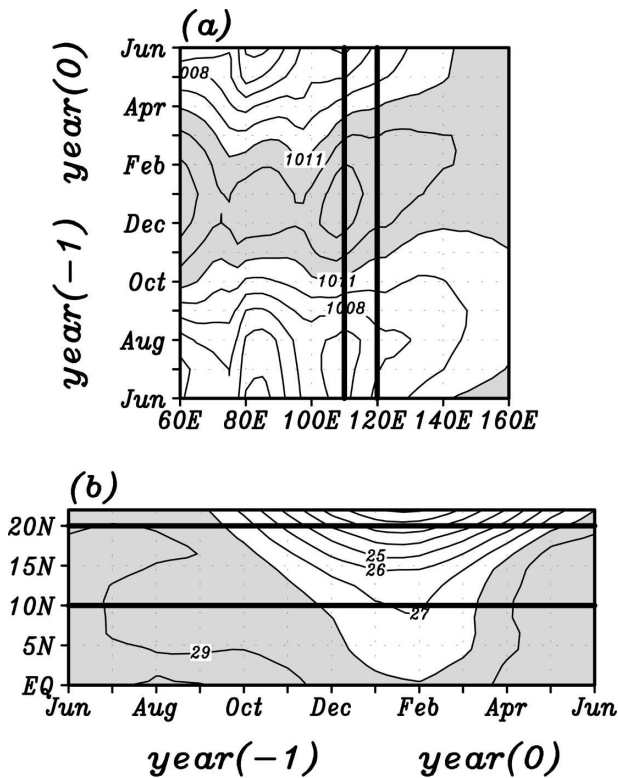
FIG. 1. Climatological annual cycles of (a) SLP averaging from the 10° to 20°N zone and of (b) SST averaging from the 110° to 120°E zone. In (a) contour intervals are 1.5 mb and SLP values larger than 1011 mb are shaded; in (b) contour intervals are 1°C and SST values larger than 28°C are shaded. The analyzed SCS region is bounded by two thick vertical lines in (a) and by two thick horizontal lines in (b).

nual and interannual features associated with the SCS FPB are examined. Annual features over the SCS region are depicted by climatological (1950–2000) annual cycles of SLP averaging from the 10° to 20°N latitudinal zone and of SST averaging from the 110° to 120°E longitudinal zone. The SLP annual cycle (Fig. 1a) shows a pressure rise over the SCS from summer to winter, corresponding to a circulation change from a monsoon trough in summer to a pressure surge associated with the westward expansion of the Pacific subtropical high and the development of the Siberia–Mongolia high in winter (e.g., Ding 2004; Chan and Li 2004). A transition occurs in fall, characterizing a minimum east–west pressure gradient across the SCS–western Pacific regions in October. The SCS SST (Fig. 1b) is relatively warm with an annual cycle ranging from 23° to 29°C. Its meridional gradient is enhanced significantly in winter due to the intrusion of cold northeasterly monsoon flows, but becomes weak in summer under the influence of warm southwesterly monsoon flows. In the transitional fall season, no dominating monsoon flow exists in the SCS,

yielding a minimum gradient around October. These features indicate that the ocean–atmosphere over the SCS is least robust in fall as being in a transitional phase from the summer monsoon system to the winter monsoon system. The SCS FPB resembles the Pacific SPB in such a way as to occur in the minimum phase of the annual cycle of the background ocean–atmosphere.

5. Interannual anomalies associated with the FPB

The FPB of the SCS SST is readily recognizable during strong ENSO cases. We thus examine interannual anomalies of strong ENSO cases, tending to identify the possible mechanism inducing the SCS FPB. Composite difference patterns of SST anomalies (El Niño minus La Niña) during ENSO's developing and mature phases [September of year (−1) to February of year (0)] are shown in Fig. 2. Their 90% significant patterns (shaded regions) reflect the primary features of El Niño evolution. Strong and elongated warming persists in the tropical eastern Pacific, while minor cooling in the tropical western Pacific and minor warming in the Indian Ocean occurs. SST anomalies in these regions vary in strength over time, but remain unchanged in sign. The SCS SSTA, however, evolves in a different way. Its significant features include an anomalous cooling in the northern SCS during September. An anomalous warming emerges in the southern SCS in October and becomes significant in November. It extends northward to cover the entire SCS in December and stretches farther northeastward into the western North Pacific with a maximum center located to the east of Taiwan from January to February of the next year. These evolutionary features reveal that the occurrence of the SCS FPB during strong ENSO cases is connected with a rapid change in the SCS SSTA during fall, changing from one regime in summer to a sign-reversed regime in winter. Lau and Yang (1996) showed that the Pacific SPB concurred with a sign reversal in the tropical eastern Pacific SSTA during spring (in their Fig. 2a). Such a sign reversal implies a quick decrease in the anomaly's persistence, setting a favorable condition for the occurrence of a persistence barrier. Consequently, the SCS SST tends to have a persistence barrier in fall.

What causes the sign reversal of the SCS SSTA during fall? The SSTA in the SCS–tropical western Pacific regions is possibly modulated by several physical mechanisms, including remote impacts of ENSO (e.g., Klein et al. 1999; Wang et al. 2000), local atmosphere–ocean interactions (e.g., Wang et al. 2003), and oceanic response to atmospheric forcing (e.g., Wang et al. 2004). These results suggest that atmospheric variability may influence the SCS SSTA, and is a possible cause
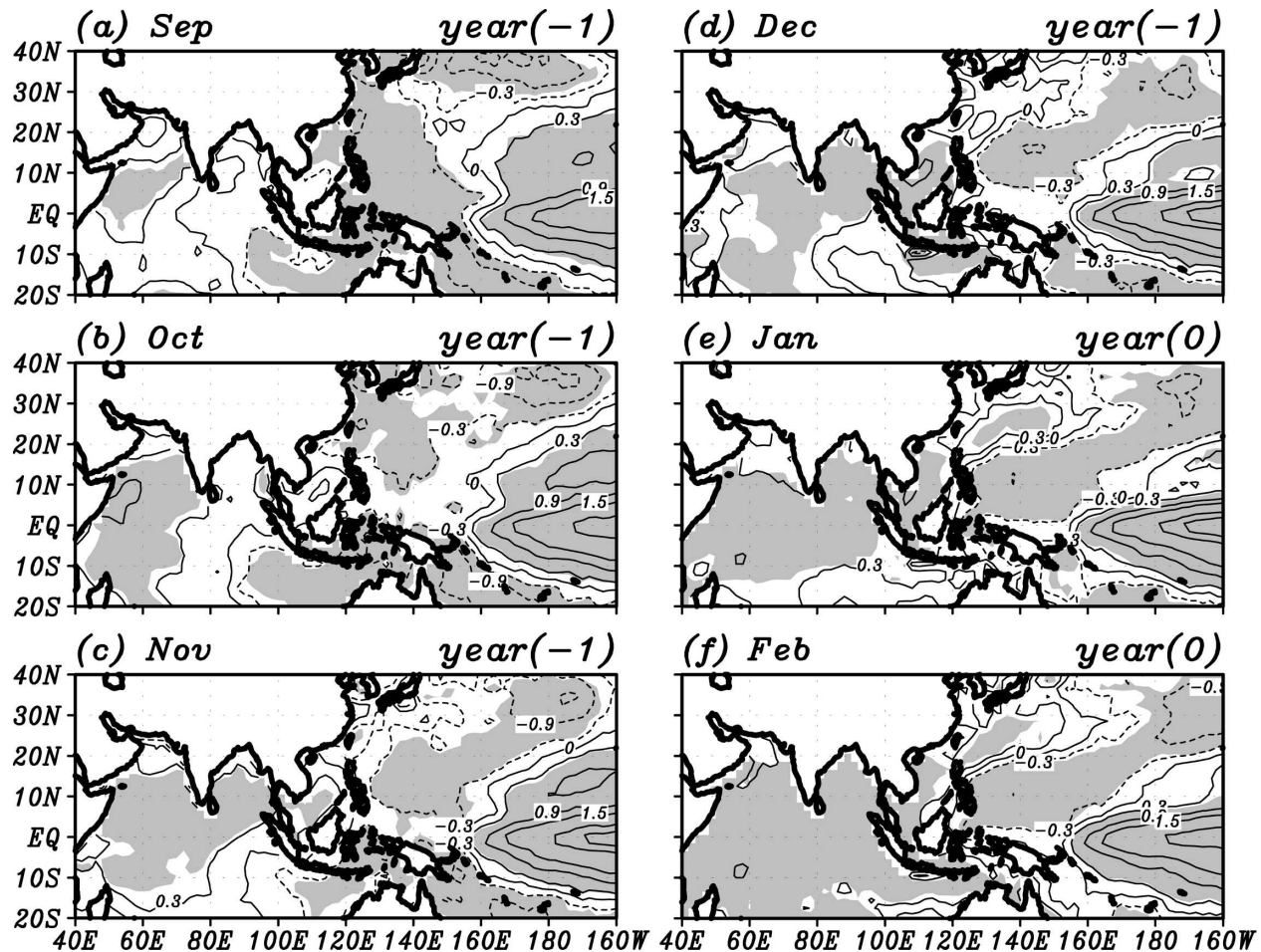
FIG. 2. Composite SST difference anomalies for strong ENSO cases (El Niño minus La Niña) during the developing and mature phases [September of year (−1) to February of year (0)]. Contour intervals are 0.3°C; anomalies significant at the 90% level are shaded.

for rapid SST changes during fall. Figure 3 shows 850-mb streamfunction (S_{850}) difference anomalies corresponding to SST difference anomalies in Fig. 2. Their significant features appear as an eastward-displacing circulation pattern characterizing the Matsuno–Gill-type pattern (Matsuno 1966; Gill 1980). In September, this circulation pattern consists of a north–south pair of elongated cyclonic anomalies straddling the equator from the Maritime Continent to the central Pacific, and a complementary pair of anticyclonic anomalies over the Arabian Sea–western Indian Ocean regions. The pair of anticyclonic anomalies intensifies and moves eastward rapidly in October and November. Its northern component moves farther eastward to center on the Philippines in December and eventually anchors in the SCS–Philippine Sea regions in the ensuing January and February. During this eastward-moving course, the SCS is under the influence of a cyclonic anomaly in September, but of an anticyclonic anomaly from October on-

ward. Figures 2 and 3 clearly show that the SCS SSTA and its overlying S_{850} anomaly both undergo a sign reversal between summer and winter. In fall, the rapid SST warming is coincident with a rapid eastward displacement of an anticyclonic anomaly into the SCS. These relationships suggest that the FPB of the SCS SST during strong ENSO cases should be closely connected with the development and evolution of a low-level circulation anomaly, which emerges in the northern Indian Ocean in early northern fall, strengthens and moves eastward along the 10°–30°N zone during fall, and eventually anchors in the Philippine Sea during northern winter.

6. Evolution of the low-level anomalous anticyclone

The low-level anticyclonic anomaly anchoring in the Philippine Sea during the winter El Niño phase is re-
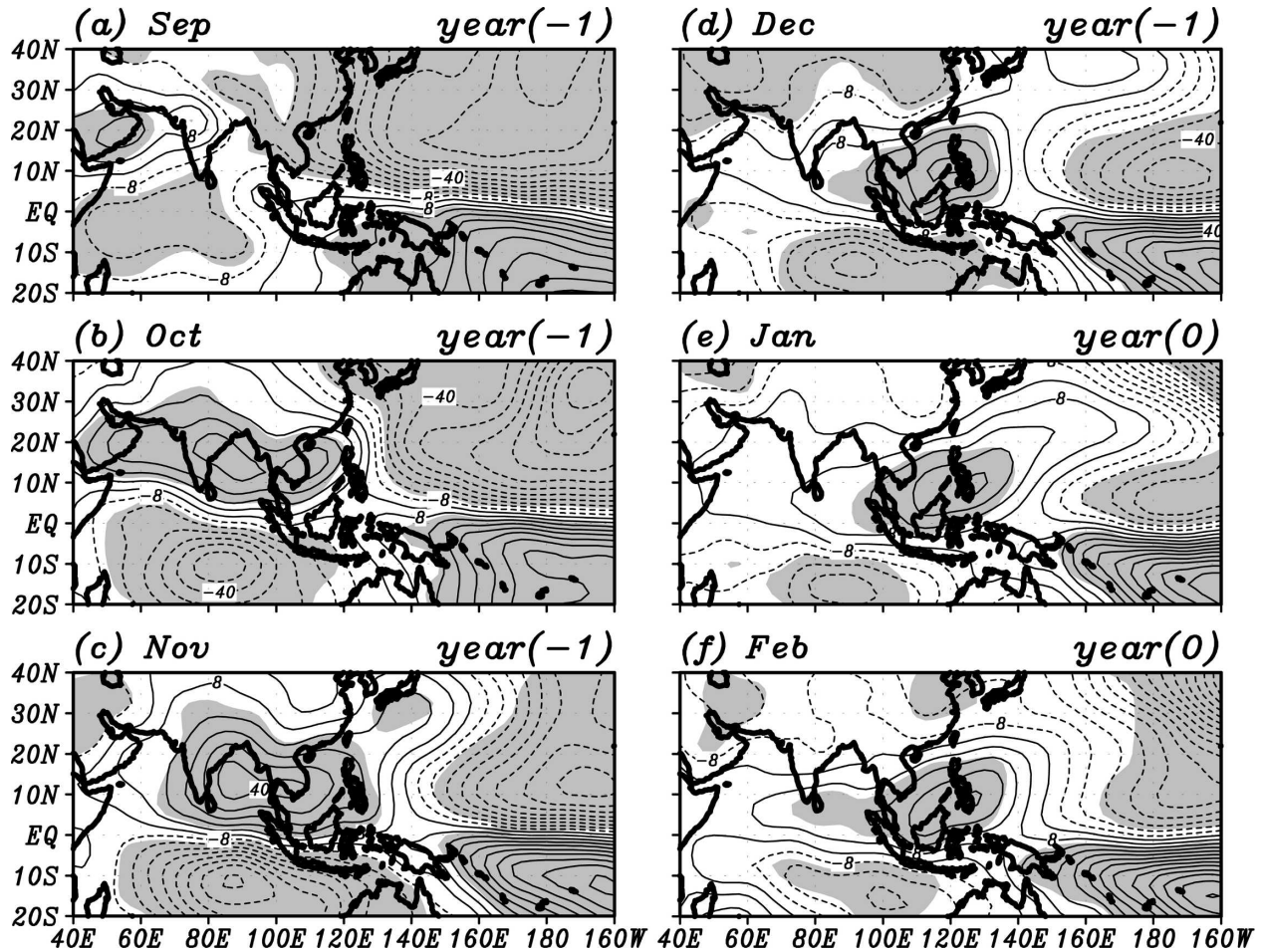
FIG. 3. As in Fig. 2 except for the 850-mb streamfunction (S_{850}) difference anomalies. Contour intervals are 8×10^5 m^2 s^{-1}; anomalies significant at the 90% level are shaded.

ferred to as the anomalous Philippine Sea anticyclone (PSAC) by Wang et al. (2000) and Wang and Zhang (2002). They noted that the anomalous PSAC forms abruptly in fall in the SCS due to two possible mechanisms: 1) remote El Niño forcing from the east and 2) extratropical–tropical interactions evoked by the midlatitude forcing from the north. Our analyses suggest a new scenario for the origin of the anomalous PSAC from the west. It is a result of the eastward displacement of a low-level anomalous anticyclone (LAAC) developing in the Indian Ocean (see Fig. 3). This displacement was suggested to be driven by a horizontal asymmetry of moisture and temperature anomalies (Chou 2004). Because the anomalous anticyclone is cold and dry in nature, its anomalous anticyclonic flows advect mean cold and dry air to its east, but warm and wet air to its west, setting an eastward-moving tendency for the anomalous anticyclone. Nevertheless, how

ENSO remotely affects this displacement remains unclear. To study this issue, composite difference anomalies of 850-mb velocity potential (X_{850}) for strong ENSO cases are shown in Fig. 4. During a strong El Niño–developing year, X_{850} anomalies contain a persistent divergent center over the Maritime Continent from September to November in response to anomalous subsidence remotely forced by the warm SSTA in the tropical central-eastern Pacific. The anomalous divergent center exhibits an axis extending from the Maritime Continent northwestward toward India in September, northward toward the East China Sea in October, and northeastward toward the western North Pacific in November, showing an eastward movement of anomalous divergence along the 10°–30°N zone. This eastward movement is concurrent with, to its west side, the intensification and eastward expansion of warm SST anomalies in the Indian Ocean (see Figs. 2a–c). This
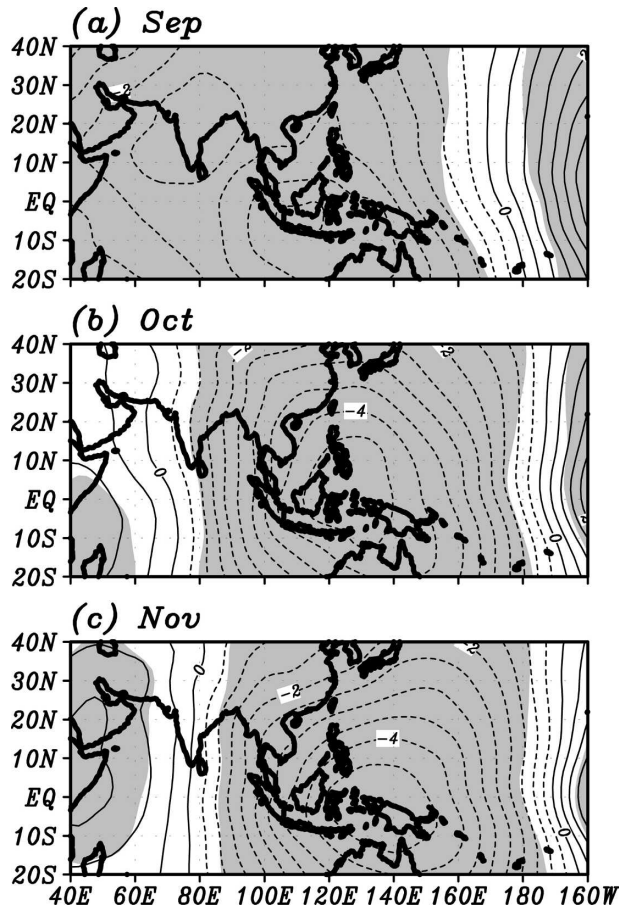
FIG. 4. As in Fig. 2 except for composite difference anomalies of 850-mb velocity potential (X_{850}) from September to November of year (−1). Contour intervals are 0.5×10^6 m² s⁻¹; anomalies significant at the 90% level are shaded.
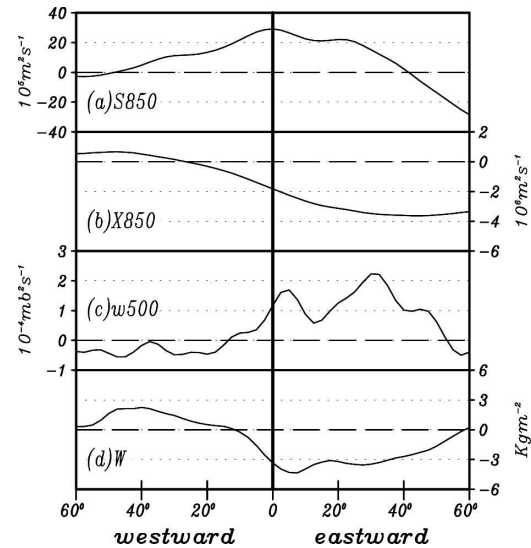

FIG. 5. Horizontal distributions of composite difference anomaly averaging from the 10°–20°N zone and over fall for (a) 850-mb streamfunction, (b) 850-mb velocity potential, (c) 500-mb vertical motion, and (d) precipitable water during strong ENSO cases. Their reference point (zero position) is the location of the maximum center of the low-level anomalous anticyclone during its eastward displacement in fall.

suggests that the developing El Niño may influence the eastward movement of the anomalous divergence via corresponding SST variability in the Indian Ocean.

To specifically portray how ENSO-induced large-scale divergence anomalies affect the LAAC's displacement, the spatial phase relationships of S_{850}, X_{850}, 500-mb vertical motion ($\omega500$), and precipitable water (W) anomalies during the eastward-displacing course are examined in Fig. 5. Their composite horizontal distributions averaging from the 10°–20°N zone and over fall are with respect to the maximum center of the LAAC (zero position in Fig. 5), which is at 55°E in September, 85°E in October, and 90°E in November (see Fig. 3). It is shown that the LAAC (positive S_{850} anomaly) is accompanied by an anomalous large-scale divergence (negative X_{850} anomaly) to its east. This anomalous divergence is accompanied with anomalous downward motion (positive ω_{500} anomaly) to suppress convective activities, yielding negative W anomaly and anomalous

dry condition. The X_{850}, ω_{500}, and W anomalies contain the opposite sign in the regions west of the LAAC. These spatial phase relationships reveal the existence of anomalous dry and divergent conditions ahead of the LAAC to facilitate its eastward movement. This result suggests that a strong ENSO acts to force the LAAC's eastward displacement via its accompanying large-scale divergence anomalies.

After the LAAC enters the Philippine Sea in winter, it is sustained and trapped in this region until the ensuing spring or early summer (e.g., Wang et al. 2000, 2004). This phenomenon was rationalized by a positive thermodynamic ocean–atmosphere feedback proposed by Wang et al. (2000). In winter, the LAAC is sandwiched by cold SST anomalies to its east over the tropical western Pacific and warm SST anomalies to its west over the SCS and Indian Ocean (see Fig. 2). With the presence of the prevailing northeasterly monsoon flows or trade winds, its anomalous anticyclonic flows intensify total wind speed to its east, maintaining the underlying cold SST anomalies through increased evaporative cooling. The cold SST anomalies, in turn, excite descending atmospheric Rossby waves that reinforce the LAAC in their westward decaying journey. As the seasonal cycle progresses, this feedback diminishes in coherence with a weakening in winter flows, leading to a gradual decay of the LAAC during the following spring and summer.
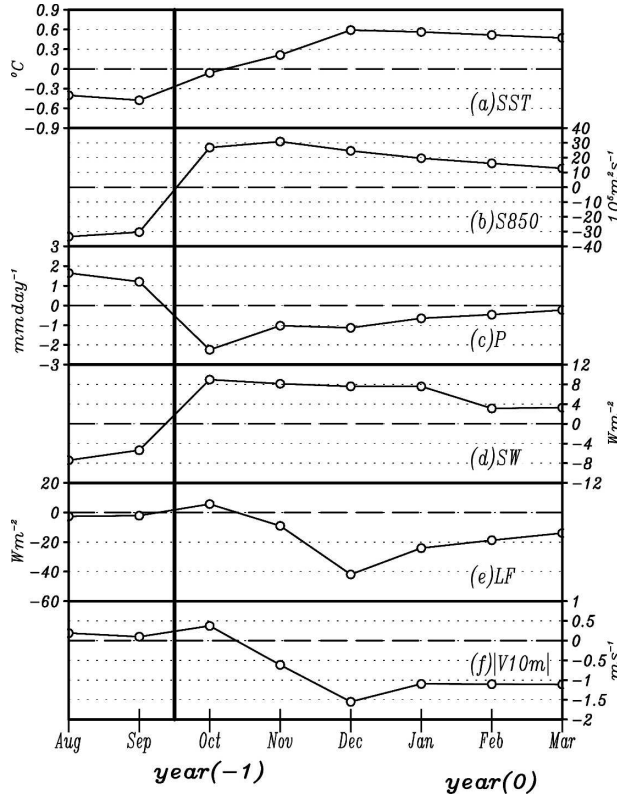
FIG. 6. As in Fig. 2 except for the anomalous area-mean fields (averaging from the domain 10°–20°N, 110°–120°E) involved in the ocean–atmosphere interaction processes over the SCS region: (a) SST, (b) S_{850}, (c) precipitation rate (P), (d) net downward shortwave radiation (SW) at the surface, (e) latent heat flux (LF) from ocean to atmosphere, and (f) total wind speed at 10 m ($|V_{10m}|$).

7. Ocean–atmosphere processes responsible for the change of the SCS SST

The eastward passage of the LAAC across the SCS induces rapid changes in the underlying SSTs during fall. What is the relative role of dynamic and thermodynamic processes in causing the SST change? The specific ocean–atmosphere processes over the SCS are investigated in terms of a surface heat budget for an area-averaged SST index (10°–20°N, 110°–120°E). Composite difference anomalies of various area-mean fields for strong ENSO cases are displayed in Fig. 6. During year (-1) of strong El Niño cases, the SCS SSTA (Fig. 6a) undergoes a rapid and continuous warming from September to December. This warming is accompanied by abrupt changes in the S_{850} anomaly (Fig. 6b) from anomalous cyclone (negative value) in September to anomalous anticyclone (positive value) in October and the later months. From October, the anomalous anticyclone effectively suppresses rainfall

activity, resulting in decreased precipitation (Fig. 6c) and enhanced net downward shortwave (SW) radiation at the surface (Fig. 6d) to warm the SCS SST. The increase in SW is evident from September to October in association with the first intrusion of the LAAC into the SCS (see Fig. 3). Meanwhile, latent heat flux (LF) from the ocean to atmosphere (Fig. 6e) hardly varies from September to October, but decreases significantly from October to December in accordance with a reduction in total wind speed at 10 m (Fig. 6f). An inspection of anomalous S_{850} patterns in Fig. 3 discloses that the prevailing winter northeasterly flows over the northern SCS are weakened in November by anomalous westerly flows from the eastern boundary of the LAAC centering in the Bay of Bengal, but in December by anomalous southwesterly flows from the western boundary of the LAAC centering in the Philippines. Temporal features of Figs. 6a, 6d, and 6e reveal that rapid SST warming from October to December is more consistent with the rapid and significant LF decreases than the minor SW increases. On the other hand, SST warming from September to October is positively enhanced by SW increases, but negatively by LF increases. The LF and SW are two dominant terms determining the surface heat budget over the tropical oceans (e.g., Hartmann and Michelsen 1993; Kitoh et al. 1999; Chen et al. 2003). The above analyses suggest two possible mechanisms for rapid SST warming in the SCS during the strong El Niño developing year. In October, anomalous warming is primarily caused by increased absorption of solar heating in accordance with the eastward intrusion of the LAAC into the SCS. In November and December, anomalous warming mainly results from a decrease in evaporative cooling as the prevailing winter flows are weakened by outer flows of the eastward-moving LAAC.

8. Relative importance of the monsoon and ENSO on the SCS FPB

The LAAC develops in the Indian Ocean in a period right after the Indian summer monsoon (ISM) during strong El Niño developing years. Previous studies noted that the ISM may have an active role in affecting the ensuing ENSO variability via anomalies in large-scale convection over the ISM region and associated east–west circulation over the tropical Pacific (e.g., Shukla and Paolino 1983; Barnett 1985; Yasunari 1990). This leads us to question the relative importance of the ISM and ENSO on the SCS FPB. The ISM index defined by Wang et al. (2001) [difference of 850-mb summer westerlies between a southern region (5°–15°N, 40°–80°E) and a northern region (20°–30°N, 70°–90°E)]
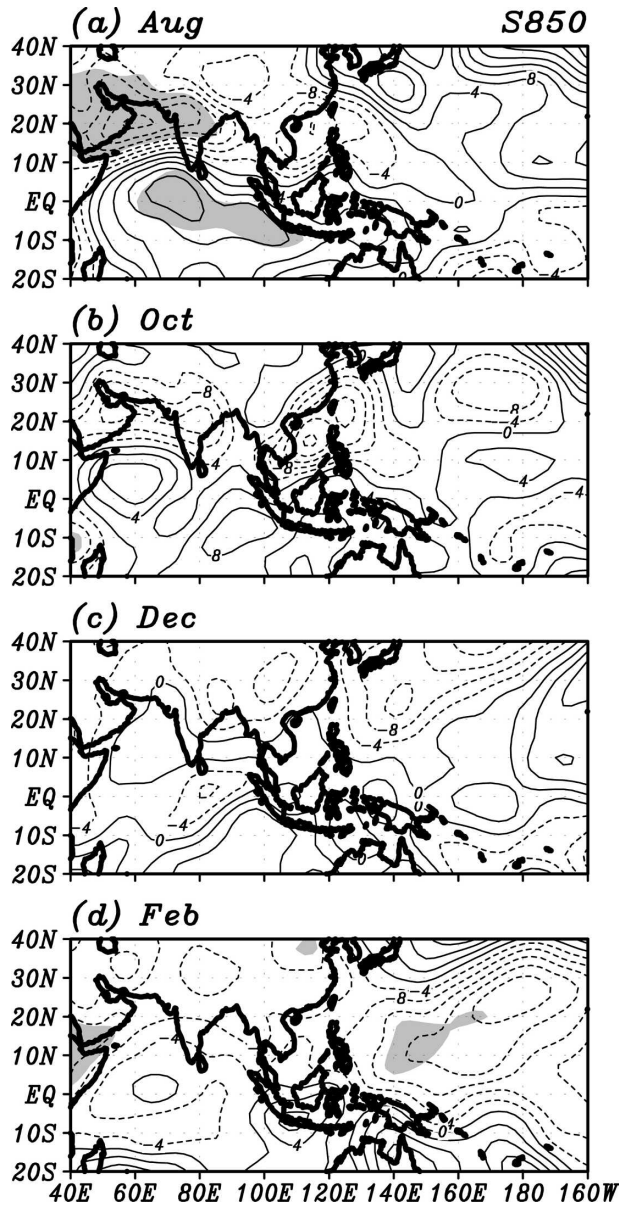
FIG. 7. Composite difference patterns of S_{850} anomalies between the strong and weak Indian summer monsoon cases (strong minus weak). Contour intervals are 4×10^5 m^2 s^{-1}; anomalies significant at the 90% level are shaded.

is used to select strong (index ≥ 1 SD) and weak (index ≤ -1 SD) ISM cases. The strong cases include the summers of 1958, 1959, 1961, 1970, 1973, 1975, 1978, 1980, and 1994 while the weak cases include the summers of 1950, 1962, 1965, 1966, 1972, 1974, 1987, and 1999. Composite difference patterns of the S_{850} anomaly between the strong and weak (strong minus weak) ISM cases are displayed in Fig. 7. It shows that the circulation anomaly does not exhibit any noticeable eastward propagation over the Indian Ocean during fall and is

not stationary in the SCS–Philippine Sea regions during winter. The lack of these two salient features indicates ISM variability as being an ineffectual factor in LAAC development. Hence, in terms of the relative importance of ENSO and ISM on LAAC development and its associated SCS FPB, it appears that ENSO is more effectual.

9. Dependence of the FPB and the LAAC on ENSO characteristics

Two issues regarding the influence of ENSO characteristics on the FPB and the LAAC are discussed. The first issue is why the FPB of the SCS SST is evident during strong ENSO cases, but becomes indiscernible during weak ENSO and normal cases. We compare the evolutionary features of SST and S_{850} anomalies among different ENSO cases in terms of their composite longitude–time patterns averaging from the 10° to 20°N zone (Fig. 8). These patterns are obtained from the differences between El Niño and La Niña cases (El Niño minus La Niña) or between positive and negative normal cases (positive minus negative). For the SST evolution, the SCS SSTA (in the 110°–120°N zone) changes from -0.4°C in August of year (-1) to 0.7°C in January of year (0) during strong ENSO cases (Fig. 8a), but from 0.1° to 0.6°C during weak ENSO cases (Fig. 8b). There is a phase reversal during fall in the former, but not in the latter. The evolution of the S_{850} anomaly (Fig. 8d) indicates the development of the LAAC as a striking feature of strong El Niño cases. A similar development seems to occur during weak El Niño cases (Fig. 8e). However, its strength is only half of its counterpart in strong El Niño cases. This result is in agreement with the Wang and Zhang (2002) finding that strength of the anomalous PSAC increases with El Niño intensity. In fact, winter SST variability, averaging over the SCS index region, is also stronger in strong ENSO cases (0.14°C) than in weak ENSO cases (0.09°C). These comparisons suggest two important factors inducing the evident SCS FPB during strong ENSO cases: 1) strong anomalies in the ocean–atmosphere and 2) a noticeable phase reversal in the SCS SSTA during fall. For normal cases (Figs. 8c and 8f), the LAAC is not developed. SST and S_{850} anomalies in the SCS are too chaotic in evolution pattern and too weak in strength, leading to an indiscernible FPB.

The second issue is regarding the effect of ENSO's longitudinal evolution on LAAC development. ENSO cases generally characterize two types of longitudinal evolution: one with major SST anomalies moving eastward from the tropical western Pacific toward the cen-
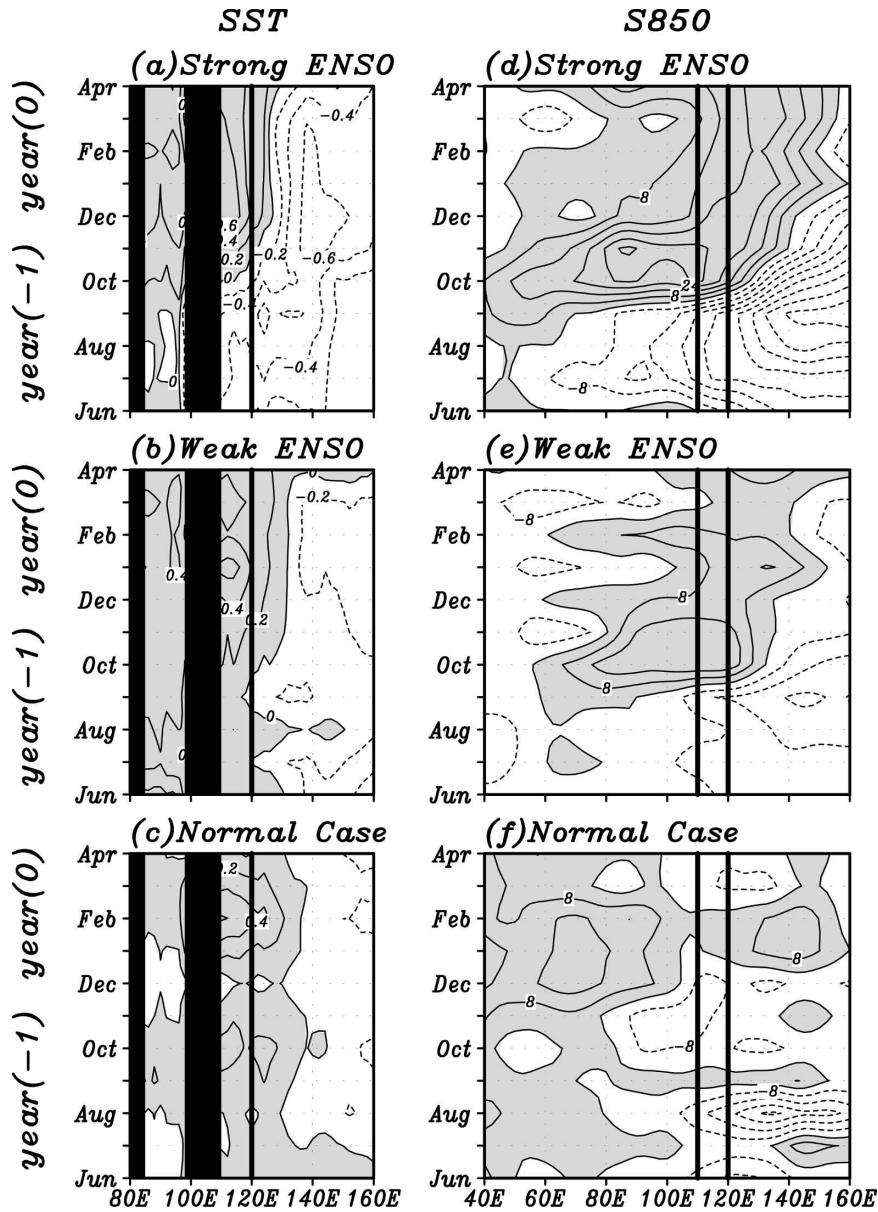
FIG. 8. Composite longitude–time patterns of SST $- S_{850}$ difference anomalies averaging from the 10°–20°N zone for (a), (d) strong ENSO (El Niño minus La Niña), (b), (e) weak ENSO (El Niño minus La Niña), and (c), (f) normal (positive minus negative) cases. Contour intervals are 0.2°C for SST anomalies and 8×10^5 m^2 s^{-1} for S_{850} anomalies. Positive values are shaded. The analyzed SCS region (110°–120°E) is bounded by two thick vertical lines.

tral-eastern Pacific and another with major SST anomalies moving westward from the eastern Pacific to the central Pacific. The former type includes the years of 1969, 1976, 1983, 1987, 1992, 1995, 1999, and 2000 while the latter type includes the years of 1955, 1956, 1958, 1966, 1971, 1973, 1974, 1978, and 1989. Composite difference patterns (El Niño minus La Niña) of S_{850} anomaly for these two ENSO types are shown in Fig. 9.

Both types exhibit the initial development of the LAAC in the Indian Ocean and its eastward movement toward the SCS. These results indicate that, while ENSO acts as a driving mechanism for LAAC development, the LAAC's eastward movement is caused mainly by local processes, regardless of the longitudinal evolutionary features of ENSO-related SSTA in the Pacific.
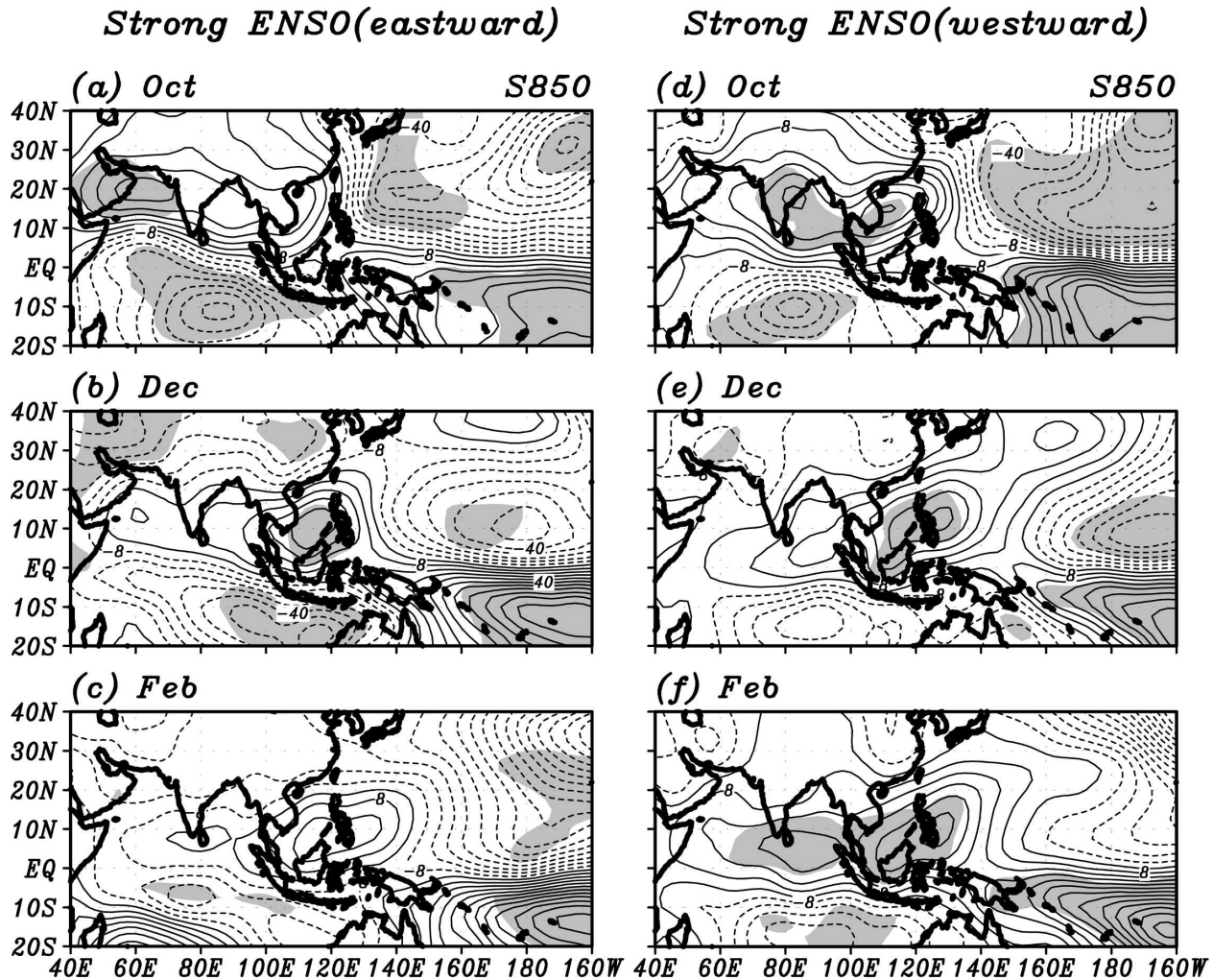
FIG. 9. Composite S_{850} difference anomalies for two types of strong ENSO cases (El Niño minus La Niña) from October of the ENSO developing year to the ensuing February: (a)–(c) ENSO's major tropical SST anomalies move eastward from the western Pacific to the central-eastern Pacific and (d)–(f) ENSO's major tropical SST anomalies move westward from the eastern Pacific to the central Pacific. Contour intervals are $8 \times 10^5 \ m^2 \ s^{-1}$; anomalies significant at the 90% level are shaded.

10. Concluding remarks

The purpose of this study is to investigate persistence characteristics of the SST anomaly (SSTA) in the South China Sea (SCS) in association with ENSO. Autocorrelations of the SCS SST index (area mean of the domain 10°–20°N, 110°–120°E) for the period 1950–2000 show a rapid and significant decrease in October and November, disclosing the existence of a fall persistence barrier (FPB) in the SCS SST. This FPB is readily recognizable during the developing phase of strong ENSO cases. In a strong El Niño event, the salient features of the SCS SSTA associated with the FPB include a phase reversal between summer and winter and a rapid warming during fall. One possible cause of these SST varia-

tions, as well as the occurrence of the FPB, is the development and evolution of a low-level anomalous anticyclone (LAAC). The LAAC emerges in the northern Indian Ocean in early northern fall, moves eastward into the SCS during fall, and eventually anchors in the Philippine Sea during northern winter. This provides a new generation scenario for the anomalous Philippine Sea anticyclone such that it originates from the Indian Ocean. The LAAC's eastward movement is apparently driven by a zonal asymmetry, relative to the anticyclonic circulation center, of divergent flow and associated atmospheric vertical motion and moisture fields. In October when the LAAC moves into the SCS, it suppresses rainfall activity, resulting in anomalous SST warming due to increased absorption of solar heating.

In November and December, outer flows of this eastward-displacing LAAC weaken the prevailing northeasterly flows over the northern SCS, leading to anomalous SST warming due to decreased evaporative cooling. The LAAC development during fall is found to be relatively independent of the preceding Indian summer monsoon and the longitudinal evolution of the ENSO-related Pacific SSTA. The above anomalies of the ocean–atmosphere contain the opposite sign in a strong La Niña event. During weak ENSO and normal cases, the key low-level circulation anomaly is either too weak in intensity or not developed, while the SCS SSTA exhibits weak intensity and no phase reversal in fall. The FPB of the SCS SST is imperceptible in these cases.

In fall, the annual cycle of the ocean–atmosphere in the SCS is at a minimum, while interannual anomalies undergo fast and striking changes during strong ENSO cases. The SCS FPB can be perceived as resulting from phase locking of interannual anomalies to the annual variation of the ocean–atmosphere, resembling the salient feature of the Pacific SPB (e.g., Lau and Yang 1996). Another marked feature in fall associated with the FPB is the eastward movement of the LAAC. Is this movement related to the eastward-moving Madden–Julian oscillation (MJO)? The MJO has a time scale of 30–60 days and propagates eastward through the globe at an average speed of $8°$ day^{-1}. The interannual anomaly LAAC has its center move from $55°E$ in September to $120°E$ in December (see Fig. 3). Its average speed is about $0.7°$ day^{-1}, only 1/10 of that for the MJO. Moreover, the LAAC becomes stationary after it reaches the SCS, while the MJO continues to propagate eastward through the whole globe. These distinctive differences suggest that the LAAC's eastward movement is irrelevant to the MJO.

The SCS SSTA undergoes a sign reversal between the periods before and after the occurrence of the FPB. This result implicates a possible connection between the FPB and the quasi-biennial oscillation (QBO) of the SCS SST (e.g., Shen and Lau 1995; Tomita and Yasunari 1996; Ose et al. 1997) or, more general, the tropical tropospheric biennial oscillation (e.g., Meehl 1997; Li et al. 2001a,b). Lau and Yang (1996) illustrated a dynamic relationship among the Pacific SPB, tropical QBO, and the summer monsoon on the quasi-biennial time scale as follows: a well-defined (vague) Pacific SPB is followed by a strong (weak) Asian summer monsoon during the cold (warm) phase of the QBO of the tropical ocean–atmosphere. Their findings lead us to speculate the possible existence of a systematic relationship between the FPB and QBO of the SCS SST and the SCS summer monsoon (e.g., Chen and Chen 1995; Lau et al. 2000). Such a relationship, if it exists, has good potential for improving summer climate prediction for East Asia. For example, the winter ENSO SST may be used to predict the ensuing summer SCS SSTA (Ose et al. 1997) because this winter-to-summer period does not encounter the SCS FPB. Then, we may base upon the predicted summer SCS SSTA, its corresponding QBO phase, and the degree of FPB in the preceding fall to project the variability of the SCS summer monsoon. The monsoon-related convective anomalies induce meridionally stratified circulation patterns to regulate summer rainfall over East Asia (e.g., Huang and Sun 1992; Wang et al. 2001; Chen et al. 2005). As such, the aforementioned relationships should help us to better predict summer climate variability in East Asia. At any rate, future efforts are needed to specifically study these dynamic relationships.

REFERENCES

Barnett, T. P., 1985: Variations in near-global sea level pressure. *J. Atmos. Sci.,* **42,** 478–501.

Cane, M. A., S. C. Dolan, and S. E. Zebiak, 1986: Experimental forecasts of the 1982/83 El Niño. *Nature,* **321,** 827–832.

Chan, J. C. L., and C. Li, 2004: The East Asian winter monsoon. *East Asian Monsoon,* C.-P. Chang, Ed., World Scientific Series on Meteorology of East Asia, Vol. 2, World Scientific, 54–106.

Chen, J.-M., C.-P. Chang, and T. Li, 2003: Annual cycle of the South China Sea surface temperature using the NCEP/NCAR reanalysis. *J. Meteor. Soc. Japan,* **81,** 879–884.

——, F.-C. Lu, S.-L. Kuo, and C.-F. Shih, 2005: Summer climate variability in Taiwan and associated large-scale processes. *J. Meteor. Soc. Japan,* **83,** 499–516.

Chen, T.-C., and J.-M. Chen, 1995: An observational study of the South China Sea monsoon during the 1979 summer: Onset and life cycle. *Mon. Wea. Rev.,* **123,** 2295–2318.

Chou, C., 2004: Establishment of the low-level wind anomalies over the western North Pacific during ENSO development. *J. Climate,* **17,** 2195–2212.

Clarke, A. J., and S. Van Gorder, 1999: The connection between the boreal spring Southern Oscillation persistence barrier and biennial variability. *J. Climate,* **12,** 610–620.

Ding, Y., 2004: Seasonal march of the East-Asian summer monsoon. *East Asian Monsoon,* C.-P. Chang, Ed., World Scientific Series on Meteorology of East Asia, Vol. 2, World Scientific, 3–53.

Gill, A. E., 1980: Some simple resolutions for heat-induced tropical circulation. *Quart. J. Roy. Meteor. Soc.,* **106,** 447–462.

Goswami, B. N., and J. Shukla, 1991: Predictability of a coupled ocean–atmosphere model. *J. Climate,* **4,** 3–22.

Hartmann, D. L., and M. L. Michelsen, 1993: Large-scale effects on the regulation of tropical sea surface temperature. *J. Climate,* **6,** 2049–2062.

Huang, R., and F. Sun, 1992: Impacts of the tropical western Pacific on the East Asian summer monsoon. *J. Meteor. Soc. Japan,* **70,** 243–256.

Kalnay, E., and Coauthors, 1996: The NCEP/NCAR 40-Year Reanalysis Project. *Bull. Amer. Meteor. Soc.,* **77,** 437–471.

Kitoh, A., T. Motoi, and H. Koide, 1999: SST variability and its mechanism in a coupled atmosphere–mixed layer ocean model. *J. Climate,* **12,** 1221–1239.

Klein, S. A., B. J. Soden, and N.-C. Lau, 1999: Remote sea surface temperature variations during ENSO: Evidence for a tropical atmospheric bridge. *J. Climate,* **12,** 917–932.

Lanzante, J. R., 1996: Lag relationships involving tropical sea surface temperatures. *J. Climate,* **9,** 2568–2578.

Latif, M., and N. E. Graham, 1992: How much predictive skill is contained in the thermal structure of an oceanic GCM? *J. Phys. Oceanogr.,* **22,** 951–962.

Lau, K.-M., and S. Yang, 1996: The Asian monsoon and predictability of the tropical ocean-atmosphere system. *Quart. J. Roy. Meteor. Soc.,* **122,** 945–957.

——, and Coauthors, 2000: A report of the field operations and early results of the South China Sea monsoon experiment (SCSMEX). *Bull. Amer. Meteor. Soc.,* **81,** 1261–1270.

Li, T., and B. Wang, 2005: A review on the western North Pacific monsoon: Synoptic-to-interannual variabilities. *TAO,* **16,** 285–314.

——, C.-W. Tham, and C.-P. Chang, 2001a: A coupled air–sea–monsoon oscillator for the tropospheric biennial oscillation. *J. Climate,* **14,** 752–764.

——, Y. S. Zhang, C.-P. Chang, and B. Wang, 2001b: On the relationship between Indian Ocean SST and Asian summer monsoon. *Geophys. Res. Lett.,* **28,** 2843–2846.

——, Y.-C. Tung, and J.-W. Hwu, 2005: Remote and local SST forcing in shaping Asian-Australian monsoon anomalies. *J. Meteor. Soc. Japan,* **83,** 153–167.

Matsuno, T., 1966: Quasi-geostrophic motions in equatorial areas. *J. Meteor. Soc. Japan,* **44,** 25–43.

Meehl, G. A., 1997: The south Asian monsoon and the tropospheric biennial oscillation. *J. Climate,* **10,** 1921–1943.

——, and J. M. Arblaster, 2002: The tropospheric biennial oscillation and Asian–Australian monsoon rainfall. *J. Climate,* **15,** 722–744.

Murakami, T., 1959: The general circulation and water vapor balance over the Far East during the rainy season. *Geophys. Mag.,* **29,** 131–171.

Ose, T., Y. Song, and A. Kitoh, 1997: Sea surface temperature in the South China Sea: An index for the Asian monsoon and ENSO system. *J. Meteor. Soc. Japan,* **75,** 1091–1107.

Reynolds, R. W., and T. M. Smith, 1995: A high resolution global sea surface temperature climatology. *J. Climate,* **8,** 1572–1583.

Shen, S., and K.-M. Lau, 1995: Biennial oscillation associated with the East Asian summer monsoon and tropical sea surface temperature. *J. Meteor. Soc. Japan,* **73,** 105–124.

Shukla, J., and D. A. Paolino, 1983: The southern oscillation and long-rang forecasting of the summer monsoon rainfall over India. *Mon. Wea. Rev.,* **111,** 1830–1837.

Smith, T. M., R. W. Reynolds, R. E. Livezey, and D. C. Stokes, 1996: Reconstruction of historical sea surface temperatures using empirical orthogonal functions. *J. Climate,* **9,** 1403–1420.

Tomita, T., and T. Yasunari, 1996: Role of the northeast winter monsoon on the biennial oscillation of the ENSO/monsoon system. *J. Meteor. Soc. Japan,* **74,** 399–413.

Wang, B., and Z. Fan, 1999: Choice of South Asian summer monsoon indices. *Bull. Amer. Meteor. Soc.,* **80,** 629–638.

——, and Q. Zhang, 2002: Pacific–East Asian teleconnetion. Part II: How the Philippine Sea anomalous anticyclone is established during El Niño development. *J. Climate,* **15,** 3252–3265.

——, R. Wu, and X. Fu, 2000: Pacific–East Asian teleconnection: How does ENSO affect East Asian climate. *J. Climate,* **13,** 1517–1536.

——, ——, and K.-M. Lau, 2001: Interannual variability of the Asian summer monsoon: Contrasts between the Indian and the western North Pacific–East Asian monsoon. *J. Climate,* **14,** 4073–4090.

——, ——, and T. Li, 2003: Atmosphere–warm ocean interaction and its impacts on Asian–Australian monsoon variations. *J. Climate,* **16,** 1195–1211.

——, I.-S. Kang, and J.-Y. Lee, 2004: Ensemble simulations of Asian–Australian monsoon variability by 11 AGCMs. *J. Climate,* **17,** 803–818.

Webster, P. J., and S. Yang, 1992: Monsoon and ENSO: Selectively interactive systems. *Quart. J. Roy. Meteor. Soc.,* **118,** 877–926.

Wright, P. B., 1984: Relationships between indices of the Southern Oscillation. *Mon. Wea. Rev.,* **112,** 1913–1919.

Yasunari, T., 1990: Impact of Indian monsoon on the coupled atmosphere/ocean system in the tropical Pacific. *Meteor. Atmos. Phys.,* **44,** 29–41.

Yu, J.-Y., 2005: Enhancement of ENSO's persistence barrier by biennial variability in a coupled atmosphere-ocean general circulation model. *Geophys. Res. Lett.,* **32,** L13707, doi:10.1029/2005GL023406.

Zebiak, S. E., and M. A. Cane, 1987: A model El Niño–Southern Oscillation. *Mon. Wea. Rev.,* **115,** 2262–2278.